Reduction of collectivity at very high spins in ^{134}Nd: Expanding the projected-shell-model basis up to 10-quasiparticle states

Long-Jun Wang,[1] Yang Sun,[1,2,3,*] Takahiro Mizusaki,[4] Makito Oi,[4] and Surja K. Ghorui[1]
[1]*Department of Physics and Astronomy, Shanghai Jiao Tong University, Shanghai 200240, China*
[2]*Collaborative Innovation Center of IFSA (CICIFSA), Shanghai Jiao Tong University, Shanghai 200240, China*
[3]*State Key Laboratory of Theoretical Physics, Institute of Theoretical Physics, Chinese Academy of Sciences, Beijing 100190, China*
[4]*Institute of Natural Sciences, Senshu University, 3-8-1 Kanda-Jinbocho, Chiyoda-ku, Tokyo 101-8425, Japan*
(Received 18 December 2015; revised manuscript received 23 February 2016; published 18 March 2016)

Background: The recently started physics campaign with the new generation of γ-ray spectrometers, "GRETINA" and "AGATA," will possibly produce many high-quality γ rays from very fast-rotating nuclei. Microscopic models are needed to understand these states.
Purpose: It is a theoretical challenge to describe high-spin states in a shell-model framework by the concept of configuration mixing. To meet the current needs, one should overcome the present limitations and vigorously extend the quasiparticle (qp) basis of the projected shell model (PSM).
Method: With the help of the recently proposed Pfaffian formulas, we apply the new algorithm and develop a new PSM code that extends the configuration space to include up to 10-qp states. The much-enlarged multi-qp space enables us to investigate the evolutional properties at very high spins in fast-rotating nuclei.
Results: We take ^{134}Nd as an example to demonstrate that the known experimental yrast and the several negative-parity side bands in this nucleus could be well described by the calculation. The variations in moment of inertia with spin are reproduced and explained in terms of successive band crossings among the 2-qp, 4-qp, 6-qp, 8-qp, and 10-qp states. Moreover, the electric quadrupole transitions in these bands are studied.
Conclusions: A pronounced decrease in the high-spin $B(E2)$ of ^{134}Nd is predicted, which suggests reduction of collectivity at very high spins because of increased level density and complex band mixing. The possibility for a potential application of the present development in the study of highly excited states in warm nuclei is mentioned.

DOI: 10.1103/PhysRevC.93.034322

I. INTRODUCTION

The concept of nuclear rotation was discovered in the early 1950s following suggestions by Bohr and Mottelson [1]. The field was quickly expanded and became a major research direction in nuclear physics, especially after the introduction of the $(\alpha,xn\gamma)$ reactions [2] and later reactions with heavy ions [3] to populate the rotational states experimentally. In the 1990s, the advanced γ-ray spectrometers for nuclear spectroscopy, "EUROBALL" [4] in Europe and "GAMMASPHERE" [5] in the United States were constructed. With the sensitivity much higher than the previous generation of instruments, these detectors played a significant role in pushing forward the entire research field of high-spin physics. With the recently started physics campaign by the yet newer generation of γ-ray spectrometers "GRETINA" [6] and "AGATA" [7] in the United States and Europe, respectively, the field is full of vigor. These facilities will allow us to extend our understanding of nuclei under extreme conditions such as the fast-rotating states in exotic nuclei with large neutron-to-proton ratios or those in superheavy nuclei.

Microscopic descriptions for the rotational motion involve coherent contributions from many nucleons. The yrast state is of particular interest because it carries valuable information of how the nucleons are organized in the lowest energy state for a given angular momentum and how the organization responds to the rotation. One of the interesting aspects in nuclei is the interplay between collective motion and single-particle degrees of freedom when nuclei are under very fast rotation [8,9]. In the ground state, nuclei tend to couple their nucleons pairwise. The introduction of the pairing correlation to nuclei [10], which is closely analogous to the superconductivity in condensed-matter physics, could successfully explain several key observations such as the odd-even staggering in nuclear binding energy, the experimental moments of inertia of deformed nuclei, the behavior of low-lying 2^+ states of even-even nuclei in the neighborhood of a closed shell, etc. [11]. In particular, pairing interaction can greatly reduce the nuclear moment of inertia, which is otherwise too large in theoretical calculations as compared to experimental data [11].

The Coriolis force, acting on the nucleon pairs in the intrinsic rotating frame, can break the pairs and thus destroy the nuclear superfluidity [12]. A sudden increase in moment of inertia at a given angular momentum (or rotational frequency ω) is usually an indication of the pair breaking in nuclei. However, an important difference between electrons in condensed matters and nucleons in nuclei is that nucleons have an orbital angular momentum in addition to spin. In a nuclear system angular momentum, j is the quantum number to work with. The nucleons in the vicinity of the Fermi surfaces in rotating nuclei belong to subshells with different j values, and therefore they feel the Coriolis force very differently. As a consequence, rotating nuclei may have a series of critical rotational frequencies, instead of one. Pairs in those orbitals with the highest j feel the strongest Coriolis force, and

*sunyang@sjtu.edu.cn

therefore break first at a low critical frequency ω_c [13]. The nucleons from the first broken pair contribute to a formation of a two-quasiparticle (qp) state as the main configuration of the yrast state, which leads to the experimentally observed back bending in moment of inertia [14]. As a nucleus rotates faster, next pair breaking can occur at a higher ω_c for the pairs from the next highest j orbitals [15], and together with the first broken pair, they can form a 4-qp state. There was reported evidence [16,17] of a successive breaking of three nucleon pairs, with 6-qp states appearing as the main configuration in the yrast sequence. When approaching the extremely high angular momentum region, it is naively expected that more pairs can break simultaneously and states with higher-order multi-quasiparticle configurations dominate the yrast structure as the main component.

Microscopic description of the above-discussed physics was a challenge. It requires a large model space with multi-qp configurations as building blocks that conserve angular momentum. There have been several beyond-mean-field methods which start from different mean fields and perform angular momentum projection to recover the rotational symmetry that is violated in the mean fields [18–24]. These methods usually focus on collective excitations of low-spin, low-excitation states by shape mixing and/or pairing mixing within the generator coordinate method, except for one recent calculation [25] that successfully included several low-order qp excitations in the model.

The projected shell model (PSM) [26] includes multi-qp configurations with angular momentum projection in the model space and thus can in principle be used to discuss physics of high-spin states. The early version of the PSM included up to 4-qp configurations in the model space of even-even nuclei and 3-qp configurations in odd-mass nuclei [26,27]. The PSM model space was extended to treat specific problems with multi-qp states [28]. A parallel extension for the projected shell model starting from a triaxially deformed basis (TPSM) also includes up to 4-qp configurations for even-even nuclei [29] and 3-qp configurations for odd-mass nuclei [30]. The reason for the basis restriction lies in the fact that, because the essential computation efforts of the PSM are to calculate the rotated matrix elements of multi-qp states using the generalized Wick's theorem [26], it would encounter a combinatorial complexity associated with practical applications when more than 4-qp states are included [31].

To overcome the bottleneck in the qp-basis extension in angular-momentum-projected theories in general, and in the PSM in particular, a breakthrough in the many-body computational method is necessary. Recently, by means of Fermion coherent states and Grassmann integral, the Pfaffian formulas were proposed [31] to calculate the rotated matrix element. The proposal was largely inspired by the initial introduction of the idea with Pfaffian by Robledo [32] to treat the sign problem in calculations of the overlap of Hartree-Fock-Bogoliubov (HFB) wave functions. It was realized later [33–37] that the method can be applied to evaluation of general HFB matrix elements. The new Pfaffian method turned out to be a feasible and very efficient algorithm for the calculations with projected multi-qp states. The first application in realistic calculation was practiced with the PSM, in which structures of the yrast band in ^{166}Hf and multi-qp high-K isomeric states in ^{176}Hf were investigated in the extended model basis that includes up to 6-qp configurations [38].

The present article reports a record extension of the qp basis with the angular-momentum-projection theory to include up to 10-qp configurations. We shall show that with this basis, high-spin states of heavy nuclei with angular momentum can reach the $I = 40 - 50\hbar$ region for the first time. With this framework, we are able to discuss rotationally induced structural changes along the yrast line in high-spin states. In our first example to see such changes, we analyze the high-spin data of ^{134}Nd and show the mechanism that generally leads to the predicted reduction of collectivity at very high spins.

The article is organized as follows. In Sec. II, we will briefly introduce the general formalism of the PSM and discuss the multi-qp basis extension. In Sec. III, the yrast band and several negative-parity side bands in ^{134}Nd, which are experimentally known up to very high spins, will be taken as an example to test the model. Electromagnetic properties of this nucleus will also be studied in this section. Finally, a summary is given in Sec. IV.

II. THEORETICAL FRAMEWORK AND BASIS EXTENSION

The PSM [26] begins with the well-established deformed Nilsson model [39] whose two parameters (the Nilsson parameters κ and μ) are empirically fitted, which gives deformed single-particle states. Pairing correlations are incorporated into these states by a BCS calculation. The Nilsson-BCS calculation defines a deformed quasiparticle basis from which the PSM model space is constructed. Then, instead of the procedure in the conventional shell model where the configurations are constructed by angular-momentum coupling, in the PSM the angular-momentum projection is carried out on those intrinsic multi-qp states to form shell-model configurations in the laboratory frame. Finally a two-body shell-model Hamiltonian is diagonalized in the projected space. The last step is the configuration mixing as in usual shell-model calculations; the difference is that the mixing is now carried out in a much smaller angular-momentum-projected basis. Note that each of the configurations in the basis is a complex mixture of multishell configurations of the spherical shell-model space. Although the final dimension of the PSM is small, it is huge in terms of original shell-model configurations. In this sense, the PSM is a shell model in a truncated multi-major-shell space.

The PSM valence space usually includes three (four) major harmonic-oscillator shells each for neutrons and protons in a calculation for normally deformed (super-deformed) nuclei. In this study, three major harmonic-oscillator shells with $N = 3,4,5$ are taken for both neutrons and protons, and the Fermi levels in such a model space lie approximately in the middle of the single-particle levels to allow a large space for particle-hole excitations.

In the present work, we restrict the configuration extension for the axially symmetric case. Let $|\Phi\rangle$ be the axially deformed qp vacuum and $a^\dagger_\nu, a^\dagger_\pi$ (a_ν, a_π) the qp creation (annihilation) operators, with the index ν (π) denoting the neutron (proton) quantum numbers. For a long period, the early version the PSM [26] used a small configuration space which included 2- and 4-qp states beyond the qp vacuum. The 4-qp states were not really the ones with four like particles, but a combination of two neutrons and two protons. Only recently, the PSM basis was expanded to include 6-qp states [38], thanks to the development of the new algorithm with the Pfaffian formulas, which enables the PSM calculation to higher spins ($I \approx 32\hbar$). In the present paper, the multi-qp configurations of the PSM (up to 10-qp states) are given for even-even nuclei as follows:

$$\begin{aligned}
&\{|\Phi\rangle,\ a^\dagger_{\nu_i}a^\dagger_{\nu_j}|\Phi\rangle,\ a^\dagger_{\pi_i}a^\dagger_{\pi_j}|\Phi\rangle,\ a^\dagger_{\nu_i}a^\dagger_{\nu_j}a^\dagger_{\pi_k}a^\dagger_{\pi_l}|\Phi\rangle,\\
&a^\dagger_{\nu_i}a^\dagger_{\nu_j}a^\dagger_{\nu_k}a^\dagger_{\nu_l}|\Phi\rangle,\ a^\dagger_{\pi_i}a^\dagger_{\pi_j}a^\dagger_{\pi_k}a^\dagger_{\pi_l}|\Phi\rangle,\\
&a^\dagger_{\nu_i}a^\dagger_{\nu_j}a^\dagger_{\nu_k}a^\dagger_{\nu_l}a^\dagger_{\nu_m}a^\dagger_{\nu_n}|\Phi\rangle,\ a^\dagger_{\pi_i}a^\dagger_{\pi_j}a^\dagger_{\pi_k}a^\dagger_{\pi_l}a^\dagger_{\pi_m}a^\dagger_{\pi_n}|\Phi\rangle,\\
&a^\dagger_{\pi_i}a^\dagger_{\pi_j}a^\dagger_{\nu_k}a^\dagger_{\nu_l}a^\dagger_{\nu_m}a^\dagger_{\nu_n}|\Phi\rangle,\ a^\dagger_{\nu_i}a^\dagger_{\nu_j}a^\dagger_{\pi_k}a^\dagger_{\pi_l}a^\dagger_{\pi_m}a^\dagger_{\pi_n}|\Phi\rangle,\\
&a^\dagger_{\pi_i}a^\dagger_{\pi_j}a^\dagger_{\nu_k}a^\dagger_{\nu_l}a^\dagger_{\nu_m}a^\dagger_{\nu_n}a^\dagger_{\nu_o}a^\dagger_{\nu_p}|\Phi\rangle, a^\dagger_{\pi_i}a^\dagger_{\pi_j}a^\dagger_{\pi_k}a^\dagger_{\pi_l}a^\dagger_{\nu_m}a^\dagger_{\nu_n}a^\dagger_{\nu_o}a^\dagger_{\nu_p}|\Phi\rangle,\\
&a^\dagger_{\pi_i}a^\dagger_{\pi_j}a^\dagger_{\pi_k}a^\dagger_{\pi_l}a^\dagger_{\nu_m}a^\dagger_{\nu_n}a^\dagger_{\nu_o}a^\dagger_{\nu_p}a^\dagger_{\nu_q}a^\dagger_{\nu_r}|\Phi\rangle,\\
&a^\dagger_{\nu_i}a^\dagger_{\nu_j}a^\dagger_{\nu_k}a^\dagger_{\nu_l}a^\dagger_{\pi_m}a^\dagger_{\pi_n}a^\dagger_{\pi_o}a^\dagger_{\pi_p}a^\dagger_{\pi_q}a^\dagger_{\pi_r}|\Phi\rangle\}. \qquad (1)
\end{aligned}$$

As the PSM works with multiple harmonic-oscillator shells for both neutrons and protons, the indices ν and π in Eq. (1) are general. For example, a 2-qp state can be of positive parity if both quasiparticles i and j are from the major N shells that differ in N by $\Delta N = 0,2,\ldots,$ or of negative parity if i and j are from those N shells that differ by $\Delta N = 1,3,\ldots$. Note that in practice, a multi-qp configuration is energetically favored when roughly half of the particles are neutrons and the other half are protons. For example, a 4-qp state $a^\dagger_\nu a^\dagger_\nu a^\dagger_\pi a^\dagger_\pi|\Phi\rangle$ with two neutrons and two protons is generally lower in energy than a 4-qp state with all like particles, $a^\dagger_\nu a^\dagger_\nu a^\dagger_\nu a^\dagger_\nu|\Phi\rangle$ or $a^\dagger_\pi a^\dagger_\pi a^\dagger_\pi a^\dagger_\pi|\Phi\rangle$, because these like particles are pushed to occupy higher-lying orbitals by mutual exclusion of the Pauli principle. Observation of a simultaneous excitation of eight or 10 like particles is practically a very rare event. Therefore, if one is interested mainly in the low excitations above the yrast line, the higher-order configurations with all like particles are not included. Consequently, for the 8- and 10-qp sectors, only two kinds of configurations are selected for each sector in the present configuration space (1).

The shell-model basis states can then be constructed with the projection technique. Without losing generality, the PSM wave function can be written as

$$\left|\Psi^\sigma_{IM}\right\rangle = \sum_{K\kappa} f^\sigma_{IK\kappa}\hat{P}^I_{MK}|\Phi_\kappa\rangle, \qquad (2)$$

where $|\Phi_\kappa\rangle$ denotes the qp basis given in Eq. (1) and $\hat{P}^I_{MK}$ the angular momentum projection operator [11],

$$\hat{P}^I_{MK} = \frac{2I+1}{8\pi^2}\int d\Omega D^I_{MK}(\Omega)\hat{R}(\Omega), \qquad (3)$$

where D^I_{MK} is the Wigner D function [40], $\hat{R}$ is the rotation operator, and Ω represents Euler angles (α, β, and γ). If one keeps the axial symmetry in the deformed basis, like in this work, D^I_{MK} in Eq. (3) reduces to the small d function and the three dimensions in Ω reduce to one only β. Note that axial symmetry implies that the set of indexes κ in the summations contains, amongst other labels, the total intrinsic magnetic quantum number K implicitly. Therefore, the summations over K are redundant because only one specific K contributes to the sum for a given κ. The energies and wave functions [expressed in terms of the coefficients $f^\sigma_{IK\kappa}$ in Eq. (2)] are obtained by solving the following eigenvalue equation:

$$\sum_{K'\kappa'}\left(H^I_{K\kappa,K'\kappa'} - E^\sigma_I N^I_{K\kappa,K'\kappa'}\right)f^\sigma_{IK'\kappa'} = 0, \qquad (4)$$

where $H^I_{K\kappa,K'\kappa'}$ and $N^I_{K\kappa,K'\kappa'}$ are, respectively, the projected matrix elements of the Hamiltonian and the norm and given by

$$\begin{aligned}
H^I_{K\kappa,K'\kappa'} &= \langle\Phi_\kappa|\hat{H}\hat{P}^I_{KK'}|\Phi_{\kappa'}\rangle,\\
N^I_{K\kappa,K'\kappa'} &= \langle\Phi_\kappa|\hat{P}^I_{KK'}|\Phi_{\kappa'}\rangle. \qquad (5)
\end{aligned}$$

These are expressed in terms of the so-called rotated matrix elements [26] which could be calculated efficiently by the Pfaffian algorithm [31,37,38], especially when states with more than four qp's are included in the basis configurations.

The PSM employs the Hamiltonian with separable forces:

$$\hat{H} = \hat{H}_0 - \frac{1}{2}\chi_{QQ}\sum_\mu \hat{Q}^\dagger_{2\mu}\hat{Q}_{2\mu} - G_M\hat{P}^\dagger\hat{P} - G_Q\sum_\mu \hat{P}^\dagger_{2\mu}\hat{P}_{2\mu}, \qquad (6)$$

where $\hat{H}_0$ is the spherical single-particle term including the spin-orbit force [41], and the rest is the quadrupole+pairing type of separable interactions, which contains three parts. The strength of the quadrupole-quadrupole force χ_{QQ} is determined in a self-consistent manner so that it is related to the deformation of the basis [26]. The monopole-pairing strength is taken according to the standard form $G_M = [G_1 \mp G_2(N-Z)/A]/A$, where "+" ("−") is for protons (neutrons), with $G_1 = 20.12$ and $G_2 = 13.13$ being the coupling constants [42,43]. The quadrupole-pairing strength G_Q is taken, as usual, to be 24% of G_M in the calculations of ^{134}Nd.

III. EXAMPLE OF HIGH-SPIN STATES IN ^{134}Nd

In Fig. 1, the calculated energy levels for ^{134}Nd are presented and compared with the experimental data. The quadrupole and hexadecapole deformation parameters are adopted as $\varepsilon_2 = 0.210$ and $\varepsilon_4 = -0.071$ to generate the deformed Nilsson single-particle basis. The value of ε_2 is taken as the experimentally suggested one [44] and ε_4 is adjusted to better reproduce the energies of the ground-state band (g band). The left column in Fig. 1 labeled as "yrast" shows the collection of theoretical levels from the lowest positive-parity state of each angular momentum, which are compared with the high-spin data of positive parity labeled "g Band" and "Band 3" in Fig. 2 of Ref. [45]. Excellent agreement is found for this yrast band up to the highest spin state. Detailed discussion about the structure evolution along the yrast line will be given below. The "yrare" band corresponds to the second lowest positive-parity states, and its main configuration at low spins is found to be $\pi 1/2^-[550] \otimes 3/2^-[541]$ with $K = 1$. The two columns in Fig. 1, both labeled "$K^\pi = 5^-$," are the levels

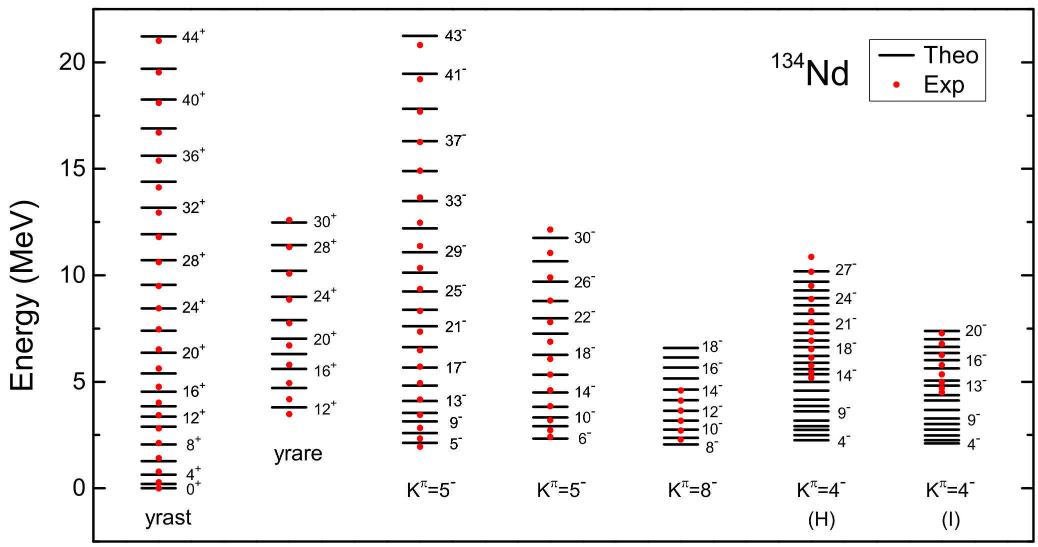

FIG. 1. Calculated energy levels for ^{134}Nd and compared with experimental data [45,46]. Following Ref. [46], we use notations (H) and (I) for the 4^- bands.

calculated for negative-parity states with the same intrinsic configuration, but plotted separately for two different signature states with even- and odd-spin numbers, respectively. Both bands have a neutron 2-qp structure at the low-spin region with the configuration $\nu 1/2^+[400] \otimes 9/2^-[514]$ and $K = 5$, which is intensively mixed with higher-order multi-qp configurations at high spins. These theoretical levels are compared with the high-spin data of negative parity labeled "Band 2" and "Band 1" in Fig. 2 of Ref. [45]. It is seen that the levels of the two bands are reproduced satisfactorily with correct positions of the band heads although there are discrepancies in the detailed level distributions. In addition to the lowest-lying negative-parity 5^- bands, other negative-parity bands labeled $K^\pi = 8^-$, 4^-(H), and 4^-(I) are also presented in Fig. 1, which are compared well with the corresponding data [46]. Among them, the two 4^- bands are the second and third lowest negative-parity bands of the calculation. At the low-spin region, these bands have the main configurations $\nu 7/2^+[404] \otimes 9/2^-[514]$ with $K = 8$, $\nu 1/2^+[400] \otimes 7/2^-[523]$ with $K = 4$, and $\nu 1/2^+[400] \otimes 9/2^-[514]$ with $K = 4$, respectively. The above results have demonstrated that the present PSM calculation can describe the data quantitatively.

Structural changes along a band can be better discussed with more sensitive plots of moment of inertia (MoI), defined as $J(I) = (2I - 1)/E_\gamma(I)$, where $E_\gamma(I) = E(I) - E(I-2)$ is the transition energy. Figure 2 shows the calculated MoI for the yrast band of ^{134}Nd in comparison with experimental data [45,46]. It is remarkable that the data can be well reproduced by the PSM for the detailed evolution with spin. As one can see from Fig. 2, the MoI undergoes drastic changes as a function of spin, changing from a very low value ($J \approx 10$ for experiment and $J \approx 15$ for theory) to $\approx$60 (all in unit $\hbar^2$ / MeV) for the highest spin state. Moreover, the overall increasing MoI is supplemented by three additional jumps. The most significant one is seen in the spin range $I = 12 \sim 14\hbar$, with a rapid increase of MoI within a small spin interval. Furthermore, there are two other clear jumps of MoI in the spin interval $20 \sim 24\hbar$ and $30 \sim 34\hbar$. Beyond $I = 34\hbar$, the MoI roughly remains constant, showing a classical rotor behavior at the high-spin region. It should be noticed that the observed rotor behavior beyond $I = 34\hbar$ cannot be described by the calculation "Theo 2" in Fig. 2 when 8- and 10-qp configurations are excluded from the configuration space (1) (see more discussions below).

Theoretical band diagrams of the PSM [26] can provide useful information for understanding the structure changes even before diagonalization is carried out. The band diagram refers to figures where energies of the theoretical bands are plotted as functions of spin. The energy of a theoretical band κ is defined as [26]

$$E_\kappa(I) = \frac{\langle \Phi_\kappa | \hat{H} \hat{P}^I_{KK} | \Phi_\kappa \rangle}{\langle \Phi_\kappa | \hat{P}^I_{KK} | \Phi_\kappa \rangle}, \tag{7}$$

which is the projected energy of a multi-qp configuration in Eq. (1). In a band diagram, the rotational behavior of each band

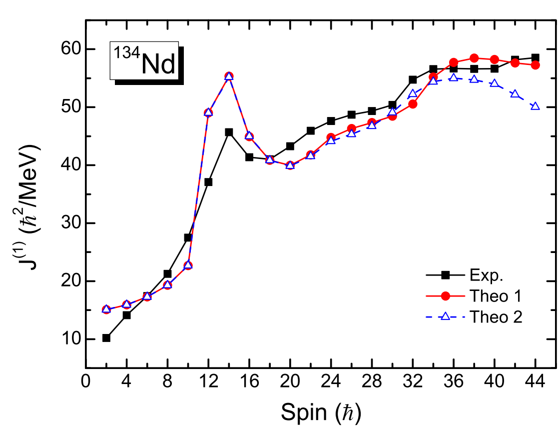

FIG. 2. Calculated moment of inertia of the yrast band for ^{134}Nd, and compared with experimental data [45,46]. The theoretical result labeled as "Theo 1" refers to the full calculation with the configuration space of (1) while "Theo 2" the one without 8- and 10-qp states.

TABLE I. The K values and configurations of bands shown in the band diagram.

Band	K	Configuration
2-qp	1	$\pi 1/2^-[550] \otimes 3/2^-[541]$
2-qp	2	$\pi 1/2^-[550] \otimes 5/2^-[532]$
4-qp	1	$\nu 7/2^-[523]9/2^-[514] \otimes \pi 3/2^-[541]3/2^-[541]$
6-qp	0, 2	$\nu 7/2^-[523]9/2^-[514] \otimes \pi 1/2^-[550]3/2^-[541]5/2^-[532]5/2^-[532]$
8-qp	2	$\nu 5/2^-[532]7/2^-[523]1/2^-[541]1/2^-[541] \otimes \pi 1/2^-[550]3/2^-[541]5/2^-[532]5/2^-[532]$
10-qp	1	$\nu 5/2^-[532]7/2^-[523]1/2^-[541]1/2^-[541] \otimes \pi 1/2^-[550]3/2^-[541]5/2^-[532]5/2^-[532] \otimes \pi 3/2^+[411]5/2^+[413]$

as well as crossings with other bands can be easily visualized. Figure 3 displays the band diagram for ^{134}Nd, where the 0-qp band (g band), two 2-qp bands, one 4-qp band, two 6-qp bands, one 8-qp band, and one 10-qp band are shown and their K values and configurations are given in Table I. These bands are selected from more than 300 projected configurations in realistic calculations because they represent the lowest bands in energy that can cross other bands and play important roles for the yrast structure evolution.

It can be seen from Fig. 3 that the proton 2-qp band with the configuration $\pi 1/2^-[550] \otimes 3/2^-[541]$ and $K = 1$ sharply crosses the g band at $I \approx 10\hbar$. This 2-qp band is further crossed at $14\hbar$ by another 2-qp band with the configuration $\pi 1/2^-[550] \otimes 5/2^-[532]$ coupled to $K = 2$. These band crossings cause sudden changes in the yrast structure, which can account for the rapid increase of MoI in the spin interval $I = 10 - 14\hbar$, as depicted in Fig. 2. We note that in many examples of rotating nuclei, particularly those in the rare-earth region, it is usually a pair of neutrons, instead of protons, to break first and align their spins to the rotation direction. It so happens because the pairs originating from higher j and smaller K orbitals are easier to be aligned by the rotation. For ^{134}Nd, the calculation shows that near the proton Fermi level, there are smaller-K orbitals ($K = 1/2$, 3/2, and 5/2) from the $h_{11/2}$ orbit. Around the neutron Fermi level, however, the nearby orbitals are $K = 7/2$ (larger K) of $h_{11/2}$ and $K = 1/2$ of $h_{9/2}$ (lower j). Therefore, proton-pair alignment is a favored process at low spins. As the nucleus rotates faster, a 4-qp band comes to approach the yrast region at about $20\hbar$. The configuration of this $K = 1$, 4-qp band is $\nu 7/2^-[523]9/2^-[514] \otimes \pi 3/2^-[541]3/2^-[541]$, which physically corresponds to a state with simultaneous breaking of one proton- and one neutron-$h_{11/2}$ pair. The 4-qp band crossing disturbs the yrast band, resulting in a smaller jump in MoI in the spin interval $I \approx 20 - 24\hbar$, as seen in Fig. 2.

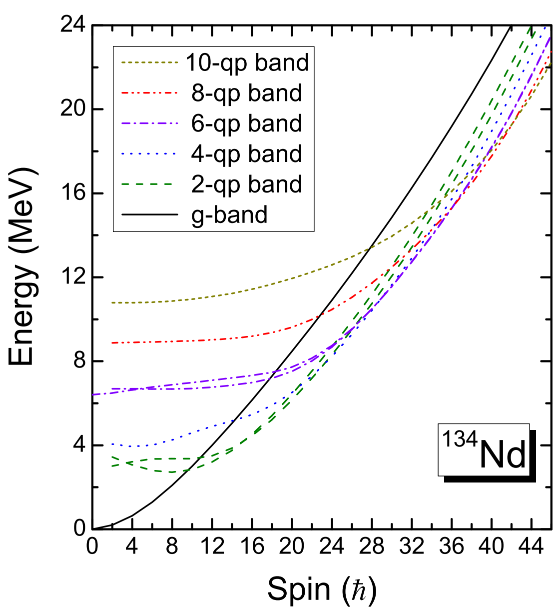

FIG. 3. Calculated band diagram (bands before configuration mixing) for the positive-parity bands near the yrast line of ^{134}Nd. See the text for details.

The 4-qp band remains to be the lowest one in energy up to $I \approx 28\hbar$. Until this spin, the yrast wave functions are relatively pure with a few dominant configurations in each state. Roughly starting from 30 $\hbar$, a more complex band-crossing picture shows up in Fig. 3. It is seen that the 4-qp band is crossed at $I \approx 30\hbar$ by two 6-qp bands almost simultaneously. The 6-qp bands are then crossed at spin $I \approx 36\hbar$ by a 8-qp band which is crossed again at $I \approx 42\hbar$ by a 10-qp band. Thus it becomes clear from Fig. 3 that the 8- and 10-qp configurations are dominant components in the wave functions with $I \geqslant 36\hbar$. It is important to note that all these crossing angles (the ratio between the slopes of two crossing bands at the crossing point; see Ref. [48] for discussion) are very small, which means that in this spin region, the different qp bands approach each other with very similar rotational frequencies (i.e., slopes of the curves in Fig. 3). Therefore the yrast states at high spins are a mixture of 4-qp, 6-qp, 8-qp, and 10-qp configurations. The effect of mixing with the highest orders of multi-qp configurations, i.e., 8- and 10-qp states, can be clearly seen in Fig. 2 by comparing the calculated results with (Theo 1) and without (Theo 2) them. Physically, these highest order qp states play a role of providing additional angular momenta to the rotating system to sustain the (roughly) constant MoI with increasing rotational frequency. The multi-qp configurations are listed in Table I.

The changes in the yrast wave functions of ^{134}Nd are expected to influence the electric quadrupole transition rate $B(E2)$, an experimental observable measuring the collectivity of nuclei. The $B(E2)$ value connecting an initial state I and a final state $I - 2$ is given by

$$B(E2, I \to I - 2) = \frac{1}{2I + 1} |\langle \Psi^{I-2} \| \hat{Q}_2 \| \Psi^I \rangle|^2, \quad (8)$$

where the wave functions $|\Psi^I\rangle$ are those in Eq. (2). The effective charges in the calculation are taken as the usual ones:

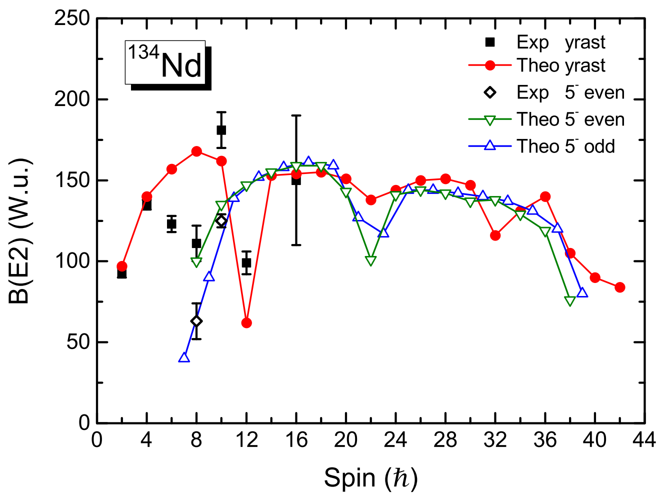

FIG. 4. Calculated $B(E2)$ values for the yrast and the negative-parity 5^- bands of ^{134}Nd, as compared with available experimental data [46,47].

$e_\pi = 1.5e$ and $e_\nu = 0.5e$. In Fig. 4, we show the calculated $B(E2)$ values for the yrast and the negative-parity 5^- bands of ^{134}Nd, and compare them with available experimental yrast data [46,47]. The results indicate that the known data could be reproduced, except for spin $I = 6$ and $8\hbar$ where an unexpected reduction in $B(E2)$ appears in the measurement that cannot be understood by the present calculation or any collective model [47]. A possible source for this discrepancy could be from the absence of triaxial deformation or the use of a basis with fixed deformation in the present work. The observed variations in the yrast $B(E2)$ at $I = 10$, 12, and $16\hbar$ are correctly reproduced by the calculation. In addition to the big drop in $B(E2)$ at $12\hbar$, reflecting the first band crossing between 0- and 2-qp states, we predict other drops at $I = 22$ and $32\hbar$, which correspond to the band crossings among the 2-qp, 4-qp, and 6-qp bands, as discussed with Fig. 3. Moreover, at the high spin region, a rapid reduction in $B(E2)$ is predicted. It is noticed that at $42\hbar$, the yrast $B(E2)$ has a value about 80 W.u., which is less than half of the highest value at $8\hbar$ ($\approx$170 W.u.). Similarly, reduced $B(E2)$ at high spins in the negative-parity 5^- bands with two different signatures is also predicted.

The most striking feature in Fig. 4 is the predicted large reduction of $B(E2)$ at high spins in ^{134}Nd. This $B(E2)$ reduction is from changes in the structure of the wave functions as higher-order qp states continuously enter into the yrast region with increasing spin. In particular, the included 8- and 10-qp configurations must play a role, as discussed previously. Experimentally, the $B(E2)$ value of the high-spin yrast band of some Yb nuclei was found to decrease significantly, indicating a significant decrease of collectivity [49–52]. It was speculated [51] that this may be from changes in the intrinsic structure of a band resulting from Coriolis effects associated with rotation. However, the calculation of $E2$-transition probabilities based on angular-momentum-projected cranked Hartree-Fock-Bogoliubov (HFB) theory [53] cannot describe the large reduction of $B(E2)$ in the high-spin region.

It is interesting that the present calculation predicts a large reduction in the high-spin $B(E2)$ suggesting a rapid decrease in deformation in the spin region where both data and calculation show an almost-constant yrast MoI. It is well known that $B(E2)$ values are sensitive essentially only to the shape and deformation, whereas MoI is sensitive to the shape but also to other properties such as alignments and pairing correlations. The shape changes suggested by the decrease in $B(E2)$ values will decrease MoI, and tend to cancel any increase from alignment. Our result with a constant MoI obtained over the range of spin but with highly mixed wave functions containing the physics of alignments and pairing supports the idea of apparently accidental cancellations.

IV. SUMMARY

In summary, the configuration space of the projected shell model is expanded to include up to 10-qp states for the first time. The Pfaffian idea initially proposed by Robledo [32] turned out to be a practical algorithm [31,37,38] for the many-body computation. This development greatly enhanced the applicability of the PSM, primarily for the states under very fast rotation. Interesting questions in high-spin physics such as the rotationally induced structural changes and the reduction of collectivity can be discussed. As the first example in application, high-spin states in ^{134}Nd are investigated. It is shown that the experimental level spectra and the moment of inertia of the yrast band can be successfully reproduced by the calculation. The observed plateau behavior of MoI at very high spins was well described and the mechanism that leads to the behavior was explained in terms of successive band crossings among 4-qp, 6-qp, 8-qp, and 10-qp states. Moreover, the electric quadrupole transition rates are calculated and compared with available data. Large reductions in high-spin $B(E2)$ were predicted for both the yrast band and the low-excited negative-parity 5^- bands, and correspondingly, reduced collectivity was discussed. Larger reductions in $B(E2)$ are suggested from our calculation because progressive changes in intrinsic structure lead to a poorer overlap between initial and final states in a transition. We expect that this is a common phenomenon in fast rotating systems and will be observed in a wide range of nuclei.

We finally remark that Fig. 3 has shown us that at the highest spin region of the current example, all rotational bands, no matter where they lie or which quasiparticle configurations they belong to, tend to rotate in a uniform manner with similar rotational frequencies ω. These bands, with different kinds of qp states and initially spreading over a large energy range in the low-spin region (roughly from 2 MeV to more than 10 MeV; see Fig. 3), are squeezed in a narrow energy window above the yrast line to form a high-level-density region with high spins. That all the qp configurations move uniformly there seems to suggest a type of collective motion emerging from the breaking of nucleon pairs. Thus the present development in PSM with the expansion to high-order multi-quasiparticle states could be a quantum-mechanical tool to understand the chaotic behavior of highly excited states [54,55] in fast-rotating nuclei, for example, the phenomenon of rotational damping [56].

ACKNOWLEDGMENTS

The authors thank G. Bertsch for encouragement and I. Ragnarsson for communication. Research at SJTU was supported by the National Natural Science Foundation of China (Grants No. 11575112 and No. 11135005), by the 973 Program of China (Grant No. 2013CB834401), and by the Open Project Program of the State Key Laboratory of Theoretical Physics, Institute of Theoretical Physics, Chinese Academy of Sciences, China (Grant No. Y5KF141CJ1).

---

[1] A. Bohr and B. R. Mottelson, K. Dan. Vidensk. Selsk. Mat. Fys. Medd. **27**, 16 (1953).
[2] H. Morinaga and P. C. Gugelot, Nucl. Phys. **46**, 210 (1963).
[3] F. S. Stephens, in *Elementary Modes of Excitation in Nuclei, Proceedings of the International School of Physics "Enrico Fermi", Course LXIX, 1976*, edited by A. Bohr and R. A. Broglia (North Holland, Amsterdam, 1977), p. 171.
[4] F. Beck, Prog. Part. Nucl. Phys. **28**, 443 (1992).
[5] I.-Y. Lee, Nucl. Phys. A **520**, C641 (1990).
[6] I.-Y. Lee, M. A. Deleplanque, and K. Vetter, Rep. Prog. Phys. **66**, 1095 (2003); I.-Y. Lee *et al.*, Nucl. Phys. A **746**, 255C (2004).
[7] S. Akkoyun *et al.*, Nucl. Instrum. Methods Phys. Res., Sect. A **668**, 26 (2012).
[8] M. J. A. de Voigt, J. Dudek, and Z. Szymański, Rev. Mod. Phys. **55**, 949 (1983).
[9] S. Frauendorf, Rev. Mod. Phys. **73**, 463 (2001).
[10] A. Bohr, B. R. Mottelson, and D. Pines, Phys. Rev. **110**, 936 (1958).
[11] P. Ring and P. Schuck, *The Nuclear Many-body Problem* (Spring-Verlag, New York, 1980).
[12] B. R. Mottelson and J. G. Valatin, Phys. Rev. Lett. **5**, 511 (1960).
[13] F. S. Stephens and R. S. Simon, Nucl. Phys. A **183**, 257 (1972).
[14] A. Johnson, H. Ryde, and J. Sztarkier, Phys. Lett. **34**, 605 (1971); A. Johnson, H. Ryde, and S. A. Hjorth, Nucl. Phys. A **179**, 753 (1972).
[15] I.-Y. Lee, M. M. Aleonard, M. A. Deleplanque, Y. El-Masri, J. O. Newton, R. S. Simon, R. M. Diamond, and F. S. Stephens, Phys. Rev. Lett. **38**, 1454 (1977).
[16] D. R. Jensen *et al.*, Eur. Phys. J. A **8**, 165 (2000).
[17] R. B. Yadav, W. C. Ma, G. B. Hagemann, H. Amro, A. Bracco, M. P. Carpenter, J. Domscheit, S. Frattini, D. J. Hartley, B. Herskind, H. Hübel, R. V. F. Janssens, T. L. Khoo, F. G. Kondev, T. Lauritsen, C. J. Lister, B. Million, S. Ødegård, L. L. Riedinger, K. A. Schmidt, S. Siem, G. Sletten, P. G. Varmette, J. N. Wilson, and Y. C. Zhang, Phys. Rev. C **80**, 064306 (2009).
[18] J. L. Egido, L. M. Robledo, and Y. Sun, Nucl. Phys. A **560**, 253 (1993).
[19] Y. Sun, L. M. Robledo, and J. L. Egido, Nucl. Phys. A **570**, 304 (1994).
[20] J. A. Sheikh and K. Hara, Phys. Rev. Lett. **82**, 3968 (1999).
[21] M. Bender and P.-H. Heenen, Phys. Rev. C **78**, 024309 (2008).
[22] J. M. Yao, J. Meng, P. Ring, and D. Pena Arteaga, Phys. Rev. C **79**, 044312 (2009).
[23] T. R. Rodríguez and J. L. Egido, Phys. Rev. C **81**, 064323 (2010).
[24] T. Niksic, D. Vretenar, and P. Ring, Phys. Rev. C **74**, 064309 (2006).
[25] B. Bally, B. Avez, M. Bender, and P.-H. Heenen, Phys. Rev. Lett. **113**, 162501 (2014).
[26] K. Hara and Y. Sun, Int. J. Mod. Phys. E **4**, 637 (1995).
[27] Y. Sun and K. Hara, Comp. Phys. Comm. **104**, 245 (1997).
[28] F.-Q. Chen, Y.-X. Liu, Y. Sun, P. M. Walker, and G. D. Dracoulis, Phys. Rev. C **85**, 024324 (2012).
[29] J. A. Sheikh, G. H. Bhat, Y. Sun, G. B. Vakil, and R. Palit, Phys. Rev. C **77**, 034313 (2008).
[30] J. A. Sheikh, G. H. Bhat, Y. Sun, and R. Palit, Phys. Lett. B **688**, 305 (2010).
[31] T. Mizusaki, M. Oi, F. Q. Chen, and Y. Sun, Phys. Lett. B **725**, 175 (2013).
[32] L. M. Robledo, Phys. Rev. C **79**, 021302(R) (2009).
[33] G. F. Bertsch and L. M. Robledo, Phys. Rev. Lett. **108**, 042505 (2012).
[34] M. Oi and T. Mizusaki, Phys. Lett. B **707**, 305 (2012).
[35] T. Mizusaki and M. Oi, Phys. Lett. B **715**, 219 (2012).
[36] B. Avez and M. Bender, Phys. Rev. C **85**, 034325 (2012).
[37] Q.-L. Hu, Z.-C. Gao, and Y. S. Chen, Phys. Lett. B **734**, 162 (2014).
[38] L.-J. Wang, F.-Q. Chen, T. Mizusaki, M. Oi, and Y. Sun, Phys. Rev. C **90**, 011303(R) (2014).
[39] S. G. Nilsson *et al.*, Nucl. Phys. A **131**, 1 (1969).
[40] D. A. Varshalovich, A. N. Moskalev, and V. K. Khersonskii, *Quantum Theory of Angular Momentum* (World Scientific, Singapore, 1988).
[41] T. Bengtsson and I. Ragnarsson, Nucl. Phys. A **436**, 14 (1985).
[42] Y. Sun and D. H. Feng, Phys. Rep. **264**, 375 (1996).
[43] P. Datta, S. Roy, S. Pal, S. Chattopadhyay, S. Bhattacharya, A. Goswami, M. Saha Sarkar, J. A. Sheikh, Y. Sun, P. V. Madhusudhana Rao, R. K. Bhowmik, R. Kumar, N. Madhavan, S. Muralithar, R. P. Singh, H. C. Jain, P. K. Joshi, and Amita, Phys. Rev. C **78**, 021306(R) (2008).
[44] R. Krücken *et al.*, Nucl. Phys. A **589**, 475 (1995).
[45] C. M. Petrache *et al.*, Phys. Lett. B **387**, 31 (1996).
[46] A. A. Sonzogni, Nucl. Data Sheets **103**, 1 (2004).
[47] T. Klemme, A. Fitzler, A. Dewald, S. Schell, S. Kasemann, R. Kühn, O. Stuch, H. Tiesler, K. O. Zell, P. von Brentano, D. Bazzacco, F. Brandolini, S. Lunardi, C. M. Petrache, C. Rossi Alvarez, G. De Angelis, P. Petkov, and R. Wyss, Phys. Rev. C **60**, 034301 (1999).
[48] K. Hara and Y. Sun, Nucl. Phys. A **529**, 445 (1991).
[49] H. Xie *et al.*, Nucl. Phys. A **599**, 560 (1996).
[50] J. C. Bacelar *et al.*, Phys. Rev. C **35**, 1170 (1987).
[51] J. C. Lisle *et al.*, Nucl. Phys. A **520**, c451 (1990).
[52] J. C. Bacelar, A. Holm, R. M. Diamond, E. M. Beck, M. A. Deleplanque, J. Draper, B. Herskind, and F. S. Stephens, Phys. Rev. Lett. **57**, 3019 (1986).
[53] K. Enami, K. Tanabe, and N. Yoshinaga, Phys. Rev. C **61**, 027301 (1999).
[54] V. Zelevinsky, B. A. Brown, N. Frazier, and M. Horoi, Phys. Rep. **276**, 85 (1996).
[55] H. A. Weidenmüller and G. E. Mitchell, Rev. Mod. Phys. **81**, 539 (2009).
[56] F. S. Stephens, M. A. Deleplanque, I. Y. Lee, D. Ward, P. Fallon, M. Cromaz, R. M. Clark, R. M. Diamond, A. O. Macchiavelli, and K. Vetter, Phys. Rev. Lett. **88**, 142501 (2002).